SCIENCE CHINA
Chemistry

• ARTICLES •
· SPECIAL TOPIC · Electrochemical Power Sources

December 2017 Vol.60 No.12:1540–1545
doi: 10.1007/s11426-017-9156-0

CeO_2@$NiCo_2O_4$ nanowire arrays on carbon textiles as high performance cathode for Li-O_2 batteries

Zhen-Dong Yang[1,2†], Zhi-Wen Chang[1,3†], Ji-Jing Xu[1], Xiao-Yang Yang[1,2] & Xin-Bo Zhang[1*]

[1]*State Key Laboratory of Rare Earth Resource Utilization, Changchun Institute of Applied Chemistry, Chinese Academy of Sciences, Changchun 130022, China*
[2]*Key Laboratory of Automobile Materials (Jilin University), Ministry of Education, Department of Materials Science and Engineering, Jilin University, Changchun 130022, China*
[3]*University of Chinese Academy of Sciences, Beijing, 100049, China*

Received August 10, 2017; accepted October 15, 2017; published online November 17, 2017

The successful development of Li-O_2 battery technology depends on developing a stable and efficient cathode. As an important step toward this goal, for the first time, we report the development of CeO_2 nanoparticles modified $NiCo_2O_4$ nanowire arrays (NWAs) grown on the carbon textiles as a new carbon-free and binder-free cathode system. In this study, the Li-O_2 battery with the CeO_2@$NiCo_2O_4$ NWAs has exhibited much reduced overpotentials, a high discharge capacity, an improved cycling stability, outperforming the Li-O_2 battery with $NiCo_2O_4$ NWAs. These improvements can be attributed to both the tailored morphology of discharge product and improved oxygen reduction reaction (ORR) and oxygen evolution reaction (OER) activity after CeO_2 NPs deposition. To a considerable extent, this idea of cathode construction including structure design and composition optimization can provide guidance for further researches in developing more powerful cathode for Li-O_2 battery.

Li-O_2 battery, efficient cathode design, CeO_2 nanoparticles, $NiCo_2O_4$ nanowire arrays, improved electrochemical performances

Citation: Yang ZD, Chang ZW, Xu JJ, Yang XY, Zhang XB. CeO_2@$NiCo_2O_4$ nanowire arrays on carbon textiles as high performance cathode for Li-O_2 batteries. *Sci China Chem*, 2017, 60: 1540–1545, doi: 10.1007/s11426-017-9156-0

1 Introduction

Rechargeable lithium-oxygen (Li-O_2) batteries have received rapidly growing attention because of their high theoretical energy density (3600 W h kg^{-1}), which is viewed as a promising alternative to gasoline [1–6]. To realize their practical application, numerous efforts have been devoted into the Li-O_2 field since the demonstrated rechargeability by Bruce in 2006 [7]. To date, great achievements in improving the performances of Li-O_2 battery have been made, however, its development is still at the infant stage. Many scientific and technological challenges, such as low round-trip efficiency, low rate capability, and a poor cycle life, need to be overcome before its final commercialization [8,9]. To address these challenges, the construction of an efficient cathode is necessary, since the cathode properties can affect the Li-O_2 reactions significantly [10].

In light of previous results, an ideal oxygen cathode requires a highly conductive and porous structure to promote the mass transfer of all reactants and house the generated Li_2O_2 [11,12]. So far, many carbonaceous cathodes with advanced architecture have been reported [13,14]. Regretfully, these carbonaceous materials can be easily degraded upon the attack of the highly oxidative oxygen species (Li_2O_2 or its intermediate LiO_2), resulting in the formation and accumulation

†These authors contributed equally to this work.
*Corresponding author (email: xbzhang@ciac.ac.cn)

of undesirable byproducts (e.g., Li_2CO_3) upon cycling that lead to performance degradation and premature battery death [15]. To get rid of this problem completely, researchers have replaced carbon with other noncarbonaceous cathode materials that are inert to these oxidative species. Till now, some suitable materials, including noble metals [16], $Ru/TiSi_2$ [17], RuO_2/NiO [18], Ru/ITO [19], Ru/STO [20], metal carbide [21], metal oxides [22,23] and transition metal oxide/carbon composite [24–26] have been used in cathodes. Despite these achieved progress, the use of these noncarbonaceous cathodes has some disadvantages. All noble metals are expensive and difficult to fabricate as a cathode. In addition, most metal oxides used in these carbon-free cathodes suffer from low electrical conductivity. It is still a daunting challenge to design a porous carbon-free cathode with low cost, high conductivity and a good electrochemical performance.

With the above understanding in mind, we speculate that a powerful carbon-free cathode for the Li-O_2 battery should possess the following properties: (1) a good conductivity for efficient electron transfer and good activity to promote the Li-O_2 reactions; (2) a reasonable structure for fast mass transfer and abundant void space to house the generated discharge products; (3) low cost and ease of fabrication, which are the premises for the massive practical application of these carbon-free cathodes in the Li-O_2 battery. To this end, we first report the efficient air cathode based on CeO_2 nanoparticles (NPs) decorated on $NiCo_2O_4$ nanowires arrays (NWAs) vertically grown on conductive carbon cloth (CC). First of all, the carbon textiles were fully covered by $NiCo_2O_4$ NWAs that the influence of carbon substrate could be ignored. Then, highly conductive $NiCo_2O_4$ NWAs act as an effective current collector that provides good electron transport [27], fast mass transfer, and sufficient void volume to house the generated Li_2O_2. Simultaneously, the $NiCo_2O_4$ NWAs also possess some oxygen reduction reaction (ORR) activity and oxygen evolution reaction (OER) activity [28]. To further improve its activity, CeO_2 NPs, which possess good ORR and OER activity [29,30], are deposited on the surface of $NiCo_2O_4$ NWAs. Finally, this Li-O_2 battery based on the CeO_2@$NiCo_2O_4$ NWAs-CC (Ce@Ni-CC) cathode demonstrates the reversible formation and decomposition of Li_2O_2, relatively low overpotentials, a high specific capacity, and high cycle stability due to its unique design in both structure and composition.

2 Experimental

2.1 Materials

Urea (99%), nickel nitrate hexahydrate ($Ni(NO_3)_2{\cdot}6H_2O$, 98%), cobalt nitrate hexahydrate ($Co(NO_3)_2{\cdot}6H_2O$, 99%), cerium nitrate hexahydrate ($Ce(NO_3)_3{\cdot}6H_2O$, 99.5%) and hexamethylenetetramine (99%) were purchased from Aladdin Reagent (China). Lithium bis(trifluoromethane sulfonyl)imide (LiTFSI) was the preferred lithium salt for all the experiments reported in this manuscript. 1 M LiTFSI in tetraethylene glycol dimethylether (TEGDME) was prepared. The water content in TEGDME electrolyte, measured by KarlFischer titration, is < 40 ppm.

2.2 Preparation of $NiCo_2O_4$ nanowires array

Carbon cloth as a substrate was sequentially cleaned by acetone, distilled water, and ethanol solution, with the assistance of sonication for 30 min each. In a typical process, a transparent pink solution was formed by dissolving 0.28 g of $Ni(NO_3)_2{\cdot}6H_2O$, 0.58 g of $Co(NO_3)_2{\cdot}6H_2O$, and 0.187 g of urea in 35 mL of H_2O at room temperature. The obtained solution was transferred into a 40 mL Teflon-lined stainless steel autoclave and put the treated carbon cloth (4 cm×4 cm) into it. Then, the autoclave was heated to 120 °C and kept at this temperature for 6 h in a conventional oven. After repeatedly rinsing with distilled water and ethanol combined with sonication, the product was dried at 80 °C in air. Finally, the Ni Co-precursor NWAs on the carbon cloth converted into well crystallized $NiCo_2O_4$ NWAs by annealing at 400 °C for 2 h.

2.3 Preparation of CeO_2@$NiCo_2O_4$ nanowires array

One piece carbon cloth (4 cm×4 cm) with $NiCo_2O_4$ NWAs was first dispersed in a mixture contained 20 mL water and 20 mL ethanol. Then, 2 mL $Ce(NO_3)_3$ aqueous solution (0.1 M) and 3 mL hexamethylenetetramine aqueous solution (HMT, 0.1 M) were added in turn, followed by a heating treatment at 70 °C for 2 h. Then the as-obtained products are washed with water and ethanol for two times.

2.4 Cell assembly

The electrochemical performance of the Li-O_2 cell was tested in a 2025-type coin cell. All of the cells were assembled in a glove box under an Ar atmosphere with a lithium metal foil anode, a glass fiber separator, an oxygen cathode and an electrolyte containing 1 M $LiCF_3SO_3$ in TEGDME. The electrode was cut into a disk with a diameter of 12 mm.

2.5 Instrumentations and characterizations

Powder X-ray diffraction (PXRD) measurements were performed on a Rigaku-MiniFlex600 power X-ray diffractometer (Japan) with Cu Kα radiation. Scanning electron microscope (SEM) was performed on a field emission Hitachi S-4800 (Japan) instrument operating at an accelerating voltage of 10 kV. Samples for SEM were prepared by dispersing the as-prepared product in ethanol by sonicating for

around 4 min and then depositing onto an indium tin oxide glass attached to an SEM brass stub. Transmission electron microscopy (TEM) was performed using an FEI Tecnai G2 S-Twin (USA) transmission electron microscope with a field emission gun operating at 200 kV. Li-O_2 cell were tested on a LAND CT2001A (China) multi-channel battery testing system.

3 Results and discussion

Figure 1(a) shows that the CeO_2@$NiCo_2O_4$ NWAs are grown vertically on the skeletons of the carbon fibers (Figure S1, Supporting Information online), forming a free-standing and porous structure. As a benefit, the problems caused by binder degradation are avoided since no polymer binder is applied. The direct growth of active materials on the carbon textile is favorable for electron transportation. The void space between these nanowires (Figure 1(b)) offers both sufficient channels to promote the mass transfer of all reactants and enough room to house the generated $L_{i2}O_2$, being beneficial to improve the performances of the Li-O_2 battery. Figure 1(c) reveals the average diameter of the nanorods is ca. 150 nm and the CeO_2 NPs are uniformly distributed along the surface of $NiCo_2O_4$ NWAs. The high-resolution TEM image collected at the surface of the $NiCo_2O_4$ NWAs (Figure 1(d)) reveals lattice fringes of ~0.31 nm in the (111) plane and ~0.27 nm in the (200) plane, demonstrating the formation of CeO_2 nanoparticles on the $NiCo_2O_4$ NWAs. Energy-dispersive X-ray spectrometry (EDXS) characterization (Figure 1(e)) further reveals the existence and homogeneous distribution of the CeO_2 NPs decorated on the surface of $NiCo_2O_4$ NWAs, indicating that the CeO_2@$NiCo_2O_4$ cathode has been well synthesized, in agreement with the XRD results. The PXRD analysis (Figure 1(f)) reveals that the diffraction peaks can be indexed to well-crystallized $NiCo_2O_4$ (PDF No. 20-0781) and CeO_2 (PDF No. 34-0394).

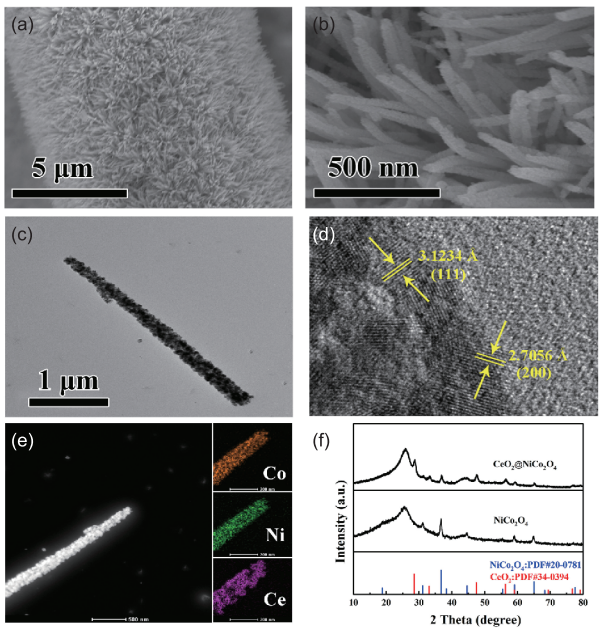

Figure 1 (a) SEM image of CeO_2@$NiCo_2O_4$ NWAs; (b) higher-magnification of (a); (c) TEM image of CeO_2@$NiCo_2O_4$ NWAs; (d) higher magnification of (c); (e) EDX-mapping analyses of CeO_2@$NiCo_2O_4$ NWAs; (f) XRD data of the as-obtained $NiCo_2O_4$ NWAs and CeO_2@$NiCo_2O_4$ NWAs (color online).

The electrochemical performances of Li-O_2 cells with Ce@Ni-CC and $NiCo_2O_4$ NWAs-CC (Ni-CC) cathodes are displayed in Figure 2. To investigate the effect of Ce@Ni-CC and Ni-CC on the ORR and OER kinetics, the first discharge-charge curves of the Li-O_2 batteries with Ce@Ni-CC and Ni-CC cathodes with the same current density (200 mA g^{-1}) are obtained, which are shown in Figure 2(a). Encouragingly, the charge overpotential of the battery with Ce@Ni-CC cathode is much lower than that of the battery with Ni-CC by about 630 mV, showing a much more facile Li_2O_2 decomposition. This excellent OER performance can be attributed to a series of unique characteristics: the added CeO_2 NPs could effectively improve the catalyst kinetics of the cathode [30]; the unique morphology of the discharge product formed on the cathode provides sufficient electrolyte-Li_2O_2 interfaces that promote the decomposition of Li_2O_2 during charge (vide infra). Simultaneously, as revealed in Figure 2(a), the discharge plateau of the battery with the Ce@Ni-CC cathode is higher than that of battery with the Ni-CC cathode by about 80 mV. This can be explained by the improved ORR activity thanks to CeO_2 deposition [31,32]. This ORR improvement agrees with the rate performance investigations, which show that the discharge voltage plateau of the Ce@Ni-CC cathode is higher than that of Ni-CC at each current density (Figure 2(b)). Furthermore, the Ce@Ni-CC cathode also demonstrates a much larger discharge capacity than the Ni-CC cathode at the same current density (Figure 2(c, d)). In light of previous report [33,34], this improvement in discharge capacity can be explained by the formation of nanosheet-like Li_2O_2 on the Ce@Ni-CC cathode rather than the muddy Li_2O_2 formed on the Ni-CC cathode. At the same time, to exclude possible electrochemical contributions from the intercalation of lithium ions (Li^+) into Ce@Ni-CC and Ni-CC materials, the initial discharge curves of Li-O_2 cells with Ce@Ni-CC and Ni-CC cathodes under an argon (Ar) atmosphere were also obtained for comparison (Figure S2). Clearly, the background discharge capacity is negligible within the voltage range, which suggests that the above obtained enhanced discharge capacities of the Li-O_2 cells are derived from the oxygen reduction.

Encouraged by the good performances achieved by Ce@Ni-CC cathode, we also investigate the cycling performance of the Li-O_2 batteries with these two cathodes shown in Figure 3(a–c); the batteries were tested by controlling the

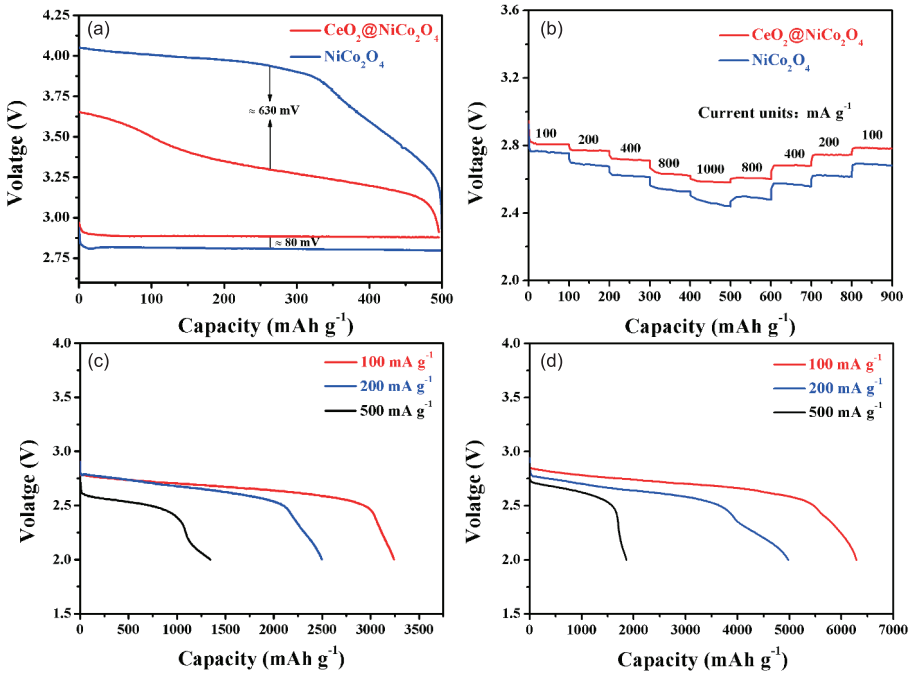

Figure 2 (a) First discharge-charge curves of Li-O_2 battery with two different cathodes (Ce@Ni-CC and Ni-CC, respectively) at a fixed capacity of 500 mA h g^{-1}; (b) the rate capability of the Li-O_2 battery with the two types of cathodes at different current densities; (c) rate performance of the battery with Ni-CC; (d) rate performance of the battery with Ce@Ni-CC (color online).

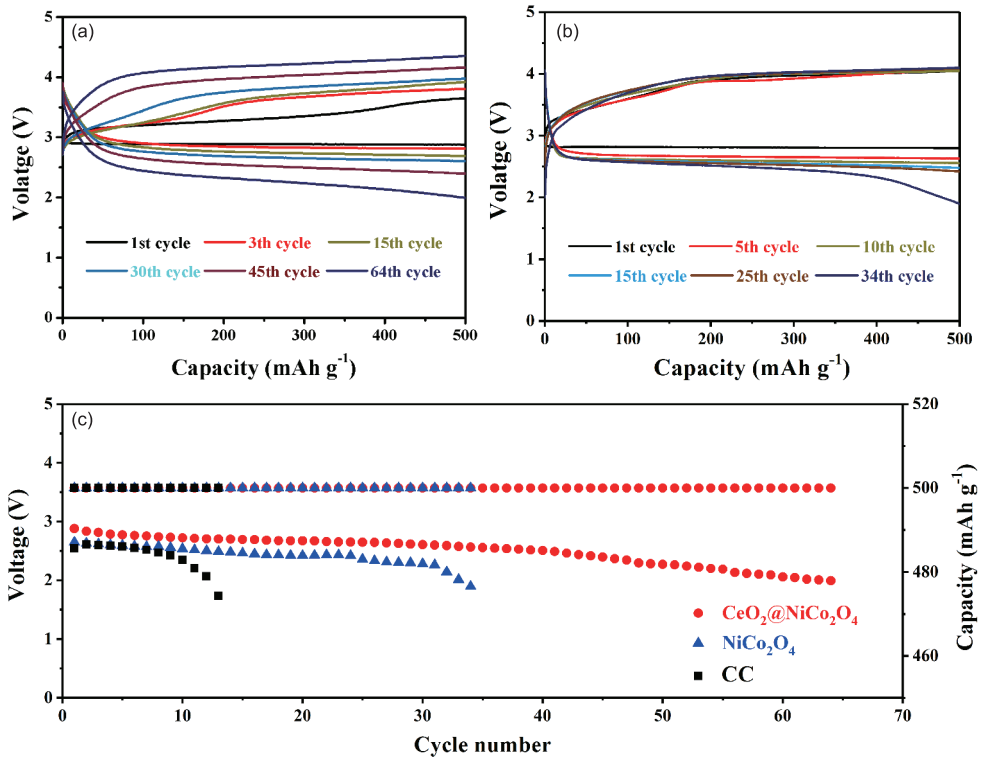

Figure 3 Cycling performance of the battery based on (a) Ce@Ni-CC cathode and (b) Ni-CC cathode with the capacity limited to 500 mA h g^{-1}; (c) variation of voltage on the terminal discharge of the Li-O_2 battery with Ce@Ni-CC (red), Ni-CC (blue) and CC (black) cathode, respectively (color online).

discharge depth to 500 mA h g^{-1} at a current density of 100 mA g^{-1}. Figure 3(a, b) shows the discharge-charge curves of these batteries based on Ce@Ni-CC and Ni-CC. Their corresponding cutoff voltages are given in Figure 3(c). As revealed, the battery with the Ce@Ni-CC cathode can discharge/charge for 64 cycles with a discharge terminal

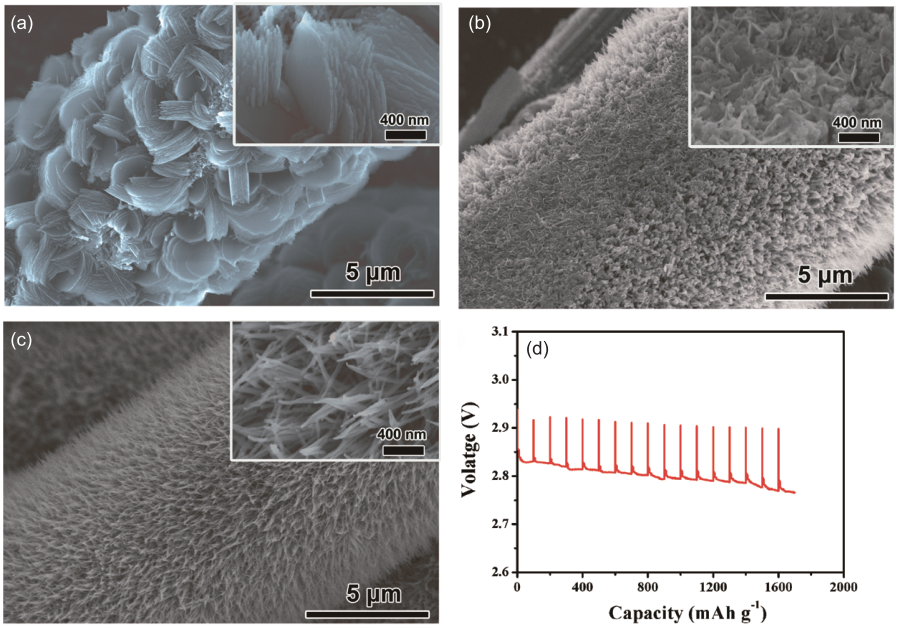

Figure 4 SEM images of the (a) Ce@Ni-CC and (b) Ni-CC cathode on first discharge, respectively. (c) SEM images of the Ce@Ni-CC cathode after recharge. These insets in the panels are the corresponding higher-magnification images. (d) GITT discharge voltage profile obtained from the Li-O_2 battery with Ce@Ni-CC cathode (color online).

voltage 2.0 V, which is much longer than the cell with the Ni-CC cathode, that is 34 cycles.

To understand the electrochemistry taking place in the Li-O_2 battery with Ce@Ni-CC cathode and Ni-CC cathode, the morphology of these discharged and charged cathodes were then investigated. Figure 4(a, b) shows the first discharged morphologies of Ce@Ni-CC cathode. Unlike the muddy discharge product formed on the Ni-CC cathode (Figure 4(b)), the discharge products formed on this cathode are nanosheets that uniformly grow vertically onto the Ce@Ni-CC cathode, indicating the formation of Li_2O_2 according to previous reports [34]. Compared with the surface of pure Ni-CC cathode, that of the Ce@Ni-CC cathode is expected to be less "sticky", which can weaken the binding of the generated superoxide to the substrate, thus enhancing the diffusion of the superoxide molecules away from the cathode surface into the electrolyte. As a benefit, the solution growth of Li_2O_2 is promoted, leading to nanosheet-shaped structure growth [34]. The uniformly and loosely distributed nanosheets provide sufficient product-electrolyte interfaces, which can promote subsequent charge process and finally enhance the electrochemical performance of the Li-O_2 battery. After recharging, the discharge product Li_2O_2 disappears and the surface of the Ce@Ni-CC cathode becomes clean again, revealing a good rechargeability of this cathode (Figure 4(c)). For further understanding the electrochemical behavior in the Li-O_2 battery, the galvanostatic intermittent titration technique (GITT) is also applied (Figure 4(d)). The equilibrium potential of the Li-O_2 battery is near 2.9 V, regardless of the state of discharge, demonstrating the formation of Li_2O_2 [35,36].

4 Conclusions

In summary, a conductive, noncarbon and binder-free cathode with CeO_2 NPs decorated on $NiCo_2O_4$ NWAs grown on the CCs is successfully constructed. When it is directly employed as an O_2 cathode, the Li-O_2 battery shows much reduced overpotentials, high discharge capacity, and enhanced cycling capability. The excellent electrochemical performance of this battery is ascribed to the reasonable 3D air cathode structure design and the homogeneous distribution of CeO_2 NPs modified on the $NiCo_2O_4$ NWAs, which has tailored the morphology of the discharged product and increased the ORR as well as OER activity. The results suggest that both the material and structure of the cathode should be optimized to achieve a Li-O_2 battery with high electrochemical performances and provide guidance for further cathode design.

Acknowledgments This work was supported by the Ministry of Science and Technology of the People's Republic of China (2017YFA0206704, 2016YFB0100103), the National Basic Research Program of China (2014CB932300), Strategic Priority Research Program of the Chinese Academy of Sciences (XDA09010404), Technology and Industry for National Defence of the People's Republic of China (JCKY2016130B010), the National Natural Science Foundation of China (51771177, 21422108, 51472232), and Jilin Province Science and Technology Development Program (20160101289JC).

Conflict of interest The authors declare that they have no conflict of interest.

Supporting information The supporting information is available online at http://chem.scichina.com and http://link.springer.com/journal/11426. The supporting materials are published as submitted, without typesetting or editing. The responsibility for scientific accuracy and content remains entirely with the authors.

1 Gao X, Chen Y, Johnson L, Bruce PG. *Nat Mater*, 2016, 15: 882–888
2 Lu J, Jung Lee Y, Luo X, Chun Lau K, Asadi M, Wang HH, Brombosz S, Wen J, Zhai D, Chen Z, Miller DJ, Sub Jeong Y, Park JB, Zak Fang Z, Kumar B, Salehi-Khojin A, Sun YK, Curtiss LA, Amine K. *Nature*, 2016, 529: 377–382
3 Jung HG, Hassoun J, Park JB, Sun YK, Scrosati B. *Nat Chem*, 2012, 4: 579–585
4 Johnson L, Li C, Liu Z, Chen Y, Freunberger SA, Ashok PC, Praveen BB, Dholakia K, Tarascon JM, Bruce PG. *Nat Chem*, 2014, 6: 1091–1099
5 Liu T, Leskes M, Yu W, Moore AJ, Zhou L, Bayley PM, Kim G, Grey CP. *Science*, 2015, 350: 530–533
6 Oh SH, Black R, Pomerantseva E, Lee JH, Nazar LF. *Nat Chem*, 2012, 4: 1004–1010
7 Ogasawara T, Débart A, Holzapfel M, Novák P, Bruce PG. *J Am Chem Soc*, 2006, 128: 1390–1393
8 Xu JJ, Wang ZL, Xu D, Meng FZ, Zhang XB. *Energ Environ Sci*, 2014, 7: 2213–2219
9 Oh D, Qi J, Lu YC, Zhang Y, Shao-Horn Y, Belcher AM. *Nat Commun*, 2013, 4: 2756
10 Chang Z, Xu J, Liu Q, Li L, Zhang X. *Adv Energ Mater*, 2015, 5: 1500633
11 Xu JJ, Xu D, Wang ZL, Wang HG, Zhang LL, Zhang XB. *Angew Chem Int Ed*, 2013, 52: 3887–3890
12 Liao K, Wang X, Sun Y, Tang D, Han M, He P, Jiang X, Zhang T, Zhou H. *Energ Environ Sci*, 2015, 8: 1992–1997
13 Lim HD, Park KY, Song H, Jang EY, Gwon H, Kim J, Kim YH, Lima MD, Ovalle Robles R, Lepró X, Baughman RH, Kang K. *Adv Mater*, 2013, 25: 1348–1352
14 Sun B, Chen S, Liu H, Wang G. *Adv Funct Mater*, 2015, 25: 4436–4444
15 Zhang T, Zhou H. *Angew Chem Int Ed*, 2012, 51: 11062–11067
16 Peng Z, Freunberger SA, Chen Y, Bruce PG. *Science*, 2012, 337: 563–566
17 Xie J, Yao X, Madden IP, Jiang DE, Chou LY, Tsung CK, Wang D. *J Am Chem Soc*, 2014, 136: 8903–8906
18 Tan P, Wei ZH, Shyy W, Zhao TS, Zhu XB. *Energ Environ Sci*, 2016, 9: 1783–1793
19 Li F, Tang DM, Chen Y, Golberg D, Kitaura H, Zhang T, Yamada A, Zhou H. *Nano Lett*, 2013, 13: 4702–4707
20 Li F, Tang DM, Jian Z, Liu D, Golberg D, Yamada A, Zhou H. *Adv Mater*, 2014, 26: 4659–4664
21 Ottakam Thotiyl MM, Freunberger SA, Peng Z, Chen Y, Liu Z, Bruce PG. *Nat Mater*, 2013, 12: 1050–1056
22 Shen C, Wen Z, Wang F, Wu T, Wu X. *ACS Catal*, 2016, 6: 4149–4153
23 Cao J, Liu S, Xie J, Zhang S, Cao G, Zhao X. *ACS Catal*, 2015, 5: 241–245
24 Tong S, Zheng M, Lu Y, Lin Z, Zhang X, He P, Zhou H. *Chem Commun*, 2015, 51: 7302–7304
25 Jiang J, He P, Tong S, Zheng M, Lin Z, Zhang X, Shi Y, Zhou H. *NPG Asia Mater*, 2016, 8: e239
26 Tong S, Zheng M, Lu Y, Lin Z, Li J, Zhang X, Shi Y, He P, Zhou H. *J Mater Chem A*, 2015, 3: 16177–16182
27 Sun B, Zhang J, Munroe P, Ahn HJ, Wang G. *Electrochem Commun*, 2013, 31: 88–91
28 Wang L, Zhu T, Lyu Z, Zhang J, Gong L, Xiao S, Liu J, Dong W, Cui X, Ho GW, Chen W. *RSC Adv*, 2016, 6: 98867–98873
29 Cao C, Xie J, Zhang S, Pan B, Cao G, Zhao X. *J Mater Chem A*, 2017, 5: 6747–6755
30 Feng JX, Ye SH, Xu H, Tong YX, Li GR. *Adv Mater*, 2016, 28: 4698–4703
31 Lin X, Zhou L, Huang T, Yu A. *Int J Electrochem Sci*, 2012, 7: 9550–9559
32 Kalubarme RS, Jadhav HS, Park CN, Jung KN, Shin KH, Park CJ. *J Mater Chem A*, 2014, 2: 13024–13032
33 Xu JJ, Chang ZW, Wang Y, Liu DP, Zhang Y, Zhang XB. *Adv Mater*, 2016, 28: 9620–9628
34 Aetukuri NB, McCloskey BD, García JM, Krupp LE, Viswanathan V, Luntz AC. *Nat Chem*, 2015, 7: 50–56
35 Lim HK, Lim HD, Park KY, Seo DH, Gwon H, Hong J, Goddard Iii WA, Kim H, Kang K. *J Am Chem Soc*, 2013, 135: 9733–9742
36 Cui ZH, Guo XX, Li H. *Energ Environ Sci*, 2015, 8: 182–187